Dissection of the components for PIP_2 activation and thermosensation in TRP channels

Sebastian Brauchi*†, Gerardo Orta*, Carolina Mascayano‡, Marcelo Salazar*, Natalia Raddatz*, Hector Urbina‡, Eduardo Rosenmann*, Fernando Gonzalez-Nilo‡, and Ramon Latorre*§

*Laboratory of Biophysics and Molecular Physiology, Centro de Estudios Cientificos, Valdivia 509-9100, Chile; ‡Centro de Bioinformatica y Simulacion Molecular Simulation Center, Universidad de Talca, Talca 346-0000, Chile

Contributed by Ramon Latorre, April 17, 2007 (sent for review March 26, 2007)

Phosphatidylinositol 4,5-bisphosphate (PIP_2) plays a central role in the activation of several transient receptor potential (TRP) channels. The role of PIP_2 on temperature gating of thermoTRP channels has not been explored in detail, and the process of temperature activation is largely unexplained. In this work, we have exchanged different segments of the C-terminal region between cold-sensitive (TRPM8) and heat-sensitive (TRPV1) channels, trying to understand the role of the segment in PIP_2 and temperature activation. A chimera in which the proximal part of the C-terminal of TRPV1 replaces an equivalent section of TRPM8 C-terminal is activated by PIP_2 and confers the phenotype of heat activation. PIP_2, but not temperature sensitivity, disappears when positively charged residues contained in the exchanged region are neutralized. Shortening the exchanged segment to a length of 11 aa produces voltage-dependent and temperature-insensitive channels. Our findings suggest the existence of different activation domains for temperature, PIP_2, and voltage. We provide an interpretation for channel–PIP_2 interaction using a full-atom molecular model of TRPV1 and PIP_2 docking analysis.

chimera | temperature activation | C-terminal domain | molecular model

Phosphatidylinositol 4,5-bisphosphate (PIP_2) acts as a second messenger phospholipid and is the source of another three lipidic-derived messengers (DAG, IP_3, PIP_3). Although the amount of PIP_2 in the membrane is very low, it is able to regulate the activity of ion channels transporters and enzymes (1–3). Several TRP channels reveal some degree of PIP_2 dependence. PIP_2 depletion inhibits TRPM7, TRPM5, TRPM8, TRPV5, and TRPM4 currents (4–9). In the case of TRPM8, some key positively charged residues present in a well conserved sequence contained in the C-terminal region of TRP channels, the TRP domain, were found to be crucial in determining the apparent affinity of PIP_2 activation (7). Residues K995, R998, and R1008 in the TRP box and TRP domain are critically involved in the activation of TRPM8 by PIP_2. The hydrolysis of PIP_2 also constitutes an important mechanism for the Ca^{2+}-dependent desensitization of TRPM8 (6, 7). Because of the high sequence similarity among TRP channels in the TRP domain region, it has been proposed that the family of TRP channels possesses a common PIP_2-binding site located on its proximal C terminus (7, 10, 11). Different from its counterparts, TRPV1 shows a PLC/NGF-dependent inhibition (12), where binding of NGF to trkA is coupled to PLC activation that leads to PIP_2 hydrolysis. Mutagenesis experiments suggested the presence of a PIP_2-dependent inhibitory domain (13). In this model, the sensitization observed in TRPV1 is explained on the basis of PIP_2 hydrolysis as it acts as a tonical inhibitor. An alternative model has been proposed for the inhibition based on NGF-dependent phosphorylation of the TRPV1 C-terminal domain and a subsequent increase in membrane expression (14). These observations, together with the finding that, in excised patches, PIP_2 activates TRPV1 (15), make uncertain the existence of a specific PIP_2-inhibitory domain.

In this article, we address the problem of PIP_2 binding and its relationship with the temperature-dependent properties of thermally sensitive TRP (thermoTRP) channels. This is an important problem to be solved because, first there is no direct evidence that positive charges present in the TRPV1 TRP domain are involved in PIP_2 activation; second, the process of temperature activation remains obscure; and third, the role of PIP_2 in such process has not been explored in detail.

Results

Unveiling Amino Acid Residues Involved in PIP_2 Activation of TRPV1. We combined the use of chimeric channels between receptors known to be responsive to cold (TRPM8) or heat (TRPV1) and site-directed mutagenesis. The main advantage of using chimeric constructs is that positive results render an exchange of phenotype. In this way, this approach provides clear structural–function answers. The coding DNA for engineered chimeras was transiently transfected in HEK-293 cells, and whole-cell patch-clamp recordings were obtained under steady-state temperature conditions. A chimera between TRPV1 and TRPM8 channels was generated, in which a cassette from the cytoplasmic C-terminal tail of hot-sensitive TRPV1 (residues V686 to W752) replaced the same C-terminal region of cold-sensitive TRPM8 (residues V982 to W1055) (Fig. 1*A*). The resultant chimera dubbed TRPM8 (686-752 V1), was sensitive to heat, voltage, and PIP_2 (Fig. 1 *B*, *C*, and *H*). TRPM8 (686-752 V1) responsiveness to PIP_2 is almost identical to the wild-type TRPM8 sensitivity to the lipid (Fig. 1*H*). In the case of TRPM8 mutations of positively charged residues contained in the TRP domain (arginines 998 and 1008; Fig. 1*A*) decrease the apparent affinity of PIP_2 activation. The point mutation R1008Q had the most dramatic effect decreasing PIP2 apparent affinity for the channel by ≈100-fold (7). In the TRP domain of TRPV1 we identify two charged residues (R701 and K710) that are conserved in TRPM8; these residues are included in the swapped cassette (Fig. 1*A*). When positive charges R701 and K710 were mutated by alanine, they strongly affect PIP_2-dependent activation, shifting dose–response curves to the right along the concentration axis (Fig. 1*H*). In contrast to the pattern followed by TRPM8 in which neutralization of R1008 has an effect almost one order of magnitude greater that neutralization of R998 (7), the effect on

Author contributions: S.B. and G.O. contributed equally to this work; S.B., G.O., C.M., M.S., N.R., E.R., F.G.-N., and R.L. designed research; S.B., G.O., C.M., M.S., N.R., H.U., E.R., and F.G.-N. performed research; S.B., G.O., E.R., and R.L. analyzed data; and S.B. and R.L. wrote the paper.

The authors declare no conflict of interest.

Abbreviations: TRP, transient receptor potential; PIP_2, phosphatidylinositol 4,5-bisphosphate; DAG, diacyl glycerol; PLC, phospholipase C; POPC, phosphatidyl oleoyl phosphatidylcholine.

†To whom correspondence may be addressed at the present address: Cardiovascular Research, Children's Hospital Harvard Medical School, Enders 1310, 320 Longwood Avenue, Boston, MA 02215. E-mail: sbrauchi@enders.tch.harvard.edu.

§To whom correspondence may be addressed. E-mail: rlatorre@cecs.cl.

www.pnas.org/cgi/doi/10.1073/pnas.0703420104

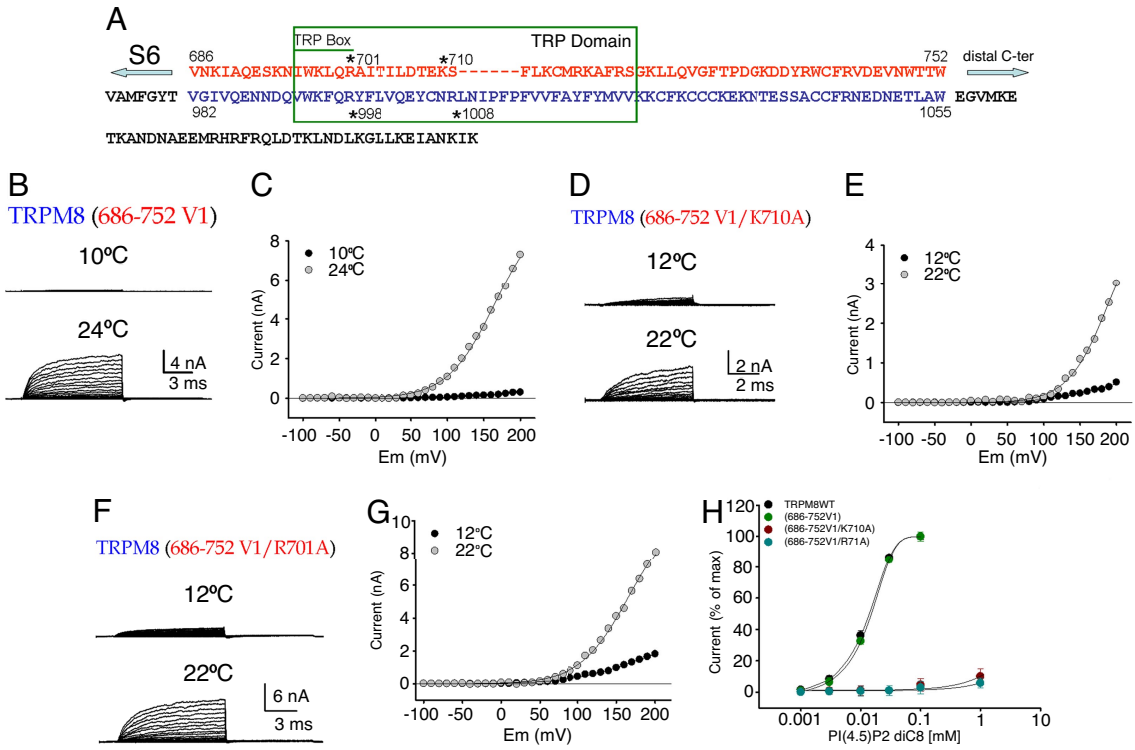

Fig. 1. PIP_2 effect is conserved among thermoTRP channel chimeras. (*A*) Schematic alignments between rTRPV1 and rTRPM8. The cut–paste limit for chimera construction is marked by different colors: blue corresponds to TRPM8 original sequence, and red corresponds to TRPV1 swapped sequence. Important features are highlighted in the scheme: the TRP domain, the TRP-box, TRPM8 charges R998 and R1008 are those involved in PIP_2 sensitivity. These charges are conserved in TRPV1 (R701 and K710). (*B*, *D*, and *F*) Representative whole-cell current recordings at two different temperatures from cells expressing TRPM8 (686-752 V1) chimera and the mutants TRPM8 (686-752 V1/K710A) and TRPM8 (686-752 V1/R701A), respectively. See *Methods* for the voltage protocol. (*C*, *E*, and *G*) Plots showing the whole-cell current as a function of voltage at the indicated temperatures for the chimeras TRPM8 (686-752 V1), TRPM8 (686-752 V1/K710A), and TRPM8 (686-752 V1/R701A), respectively. (*H*) PIP_2 Dose–response curve for WT TRPM8, TRPM8 (686-752 V1) chimera, and the mutants TRPM8 (686-752 V1/K710A) and TRPM8 (686-752 V1/R701A). Curves were fitted to a Hill equation (solid lines). A Hill coefficient of 1.2 was obtained for WT TRPM8 and TRPM8 (686-752 V1) chimera. Each point represents an average of at least four different experiments. Error bars indicate SE.

the PIP_2 activation curve is essentially the same when K710 or R701 are mutated to alanine (Fig. 1*H*). None of the mutations abolishes the strong heat response ($Q_{10} \approx 10$; see Fig. 3*B*) observed in the chimeric channel TRPM8(686-752V1) (compare Fig. 1*C* with Fig. 1 *E* and *G*). However, we observed that the activation curve is shifted toward depolarizing potentials in the mutated chimeras (see Fig. 3*A*).

A Small Region Inside the C-Terminal Tail of TRPV1 Confers Heat Sensitivity. Additional chimeras were designed to define a minimal portion able to confer temperature sensitivity to a TRP channel (Fig. 2*A* and *B*). Our results show that the region located outside the TRP domain comprising the TRPV1 C-terminal amino acids Q727 and W752 is the minimal portion able to turn TRPM8 into a heat receptor (Fig. 2 *A* and *C*). Decreasing the length of this region to <11 aa residues abolishes thermal sensitivity ($Q_{10} \approx 3$) but retains voltage dependence (Figs. 2 *B* and *F* and 3*A*). TRPM8 (741-752V1) chimeric channel (Fig. 2*B*) is essentially insensitive to temperature changes (Figs. 2*E* and 3*B*). No changes in conductance were observed between 10°C and 40°C (data not shown). Although temperature thresholds and Q_{10}s vary considerably, we notice that the voltage sensitivity remains virtually unchanged (Fig. 3*A*) when compared with the wild-type TRPM8 channels where $V_{0.5}$ at 22°C is ≈80 mV (31, 32). This observation suggested to us that the coupling between thermal activation machinery and the gate is strongly affected, whereas the voltage-sensing properties are not. This somewhat supports the argument that voltage and thermal gating are separable. As reported previously with chimeric constructs between TRPM8 and TRPV1 in which the whole C termini were exchanged, the chimeric channels described here have lower Q_{10}s than observed in wild-type channels (Fig. 3*B*). Although smaller, the Q_{10} s found (≈10) are still much larger than that found for the gating of other channels (≈3). The lower Q_{10} found may imply that the functional coupling between thermal energy and mechanical energy needed for channel opening is maintained but with a lower efficiency in the chimeric channels.

An increase in the electrical activity of both chimeras described above was observed when PIP_2 10 μM was present in the patch pipette unless R701 and K710 were altered (Fig. 3*C*). In TRPM8, residue Y745 in S2 strongly shifted the concentration-dependence of menthol activation, suggesting that this site influences menthol binding (16). Mutations in S4 also affect menthol efficacy as an activator, notably R842H, suggesting the possibility that menthol binds to the hydrophobic cleft included between domains S2 and S4 (17). Taking into account these and a previous report (18) that locate primary menthol-binding sites outside the C-terminal domain, we investigated the sensitivity of menthol-evoked responses to test proper channel function. All of the chimeras exhibited robust responses to 300 μM menthol when added to the bath solution (Fig. 3*C*). These data suggest that menthol activation involves a different mechanism than temperature and PIP_2.

Building a TRPV1 Homology Model. In the absence of high-resolution TRP channel structural data, we built a molecular model for TRPV1 to help interpret our results (Fig. 4). The homology model was built using the crystal structures of Kv1.2

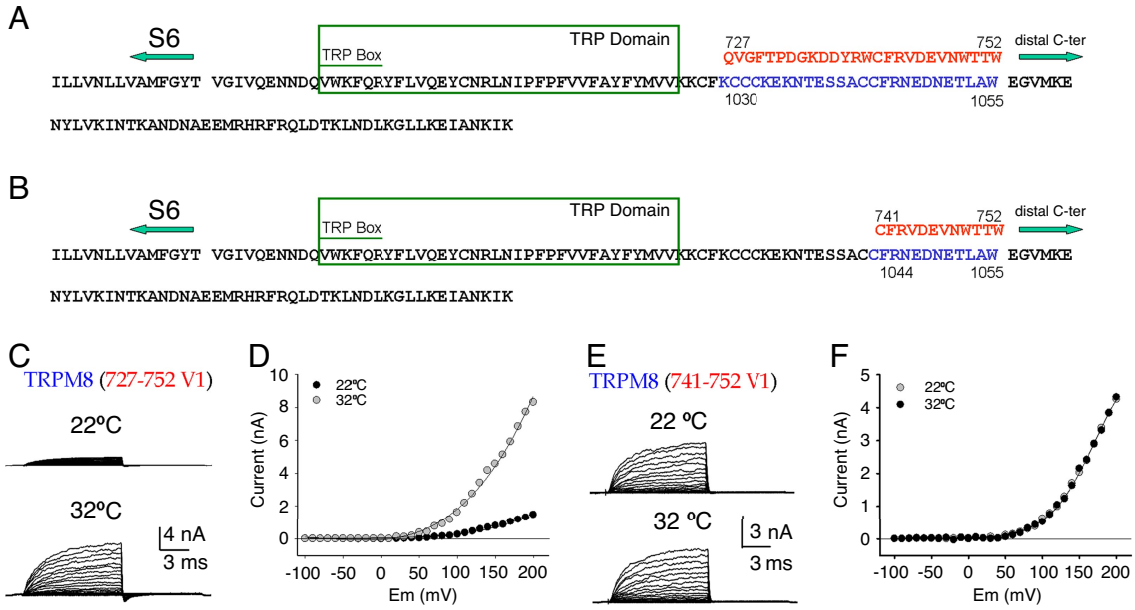

Fig. 2. A small region inside the C-terminal tail of TRPV1 confers heat sensitivity. (*A* and *B*) Schematic alignments between rTRPV1 and rTRPM8. The cut–paste limit for chimera construction is marked by different colors, and the corresponding amino acid number for each sequence boundaries is highlighted. (*C* and *E*) Representative whole-cell recordings of cells expressing TRPM8 (727-752 V1) and TRPM8 (741-752 V1) chimeras, respectively. Cells were exposed to different temperatures to compare their heat responsiveness. See *Methods* for the voltage protocol. (*D*) Whole-cell current as a function of voltage at the indicated temperatures for TRPM8 (727-752 V1) chimera. (*F*) Whole-cell current as a function of voltage at the indicated temperatures for TRPM8 (741-752 V1) chimera. This 11-aa chimera lacks the temperature responsiveness but retains voltage dependence.

(19) and HCN2 (20) as templates for membrane and C-terminal regions, respectively. The model was embedded into an explicit phosphatidyl oleoyl phsophatidylcholine (POPC) membrane and relaxed using a full-atom molecular-dynamics simulation (Fig. 4*A*). Several docking grids were used to explore the PIP_2-binding site, and our analysis consistently place PIP_2 aliphatic chains near to the voltage-sensor modules. The results of the docking simulation place the PIP_2 polar head interacting with a cluster of positive charges located in the proximal C-terminal region (Fig. 4*B*). The full molecular system that includes TRPV1 channel, PIP_2 molecules, POPC membrane, explicit water, and counter ions, was stable through 5 ns of molecular-dynamics simulation. During the trajectory, several salt bridges reorganize, forming intersubunit interactions providing stability to the proximal C-terminal region. After the molecular simulation, the PIP_2 polar head appeared making periodic contact with positive charges K694, K698, and K701 from the proximal C terminus and with amino acids R575 and R579 located in the S4–S5 linker (data not shown).

Discussion

A Possible PIP_2-Dependent Activation Mechanism. Molecular models have proven to be useful to understand the mechanics of ion channels and their molecular interactions (21, 22). Although there is no crystal structure available for TRP channels, nonrefined homology models for the TRPV1 pore module (23) and its C-terminal domain (24, 25) have been proposed. García-Sanz *et al.* (24) used the crystallographic structure of the C-terminal fragment of the hyperpolarized and cyclic nucleotide-gated (HCN) channel (20) as a template for modeling the TRPV1 C terminus. Structurally the tetrameric structures formed by the C termini of TRPV1 and HCN are very similar, and it is tempting to suggest that the similarity between the TRPV1 C terminus tetrameric structure with that of the same region of HCN channels implies also a likeness in function. In HCN channels, Zagotta *et al.* (19) proposed that this structure constitutes a gating ring able to transform the cyclic nucleotide-binding energy into the mechanical energy necessary to open the pore. Sequence analysis suggests that TRP channels share the architecture of Kv channels, formed by six transmembrane (TM) domain monomers (26, 27), and it has been shown that they assemble as tetramers (28, 29). In this work, we present a full-atom refined model of the TRPV1 channel. We built this model in the lack of crystallographic data from a close relative to help us visualize our results. Although the model should be taken cautiously, it proved to be extremely useful in the interpretation of our experimental results. Interestingly, our docking procedure places PIP_2 in contact with charges present in the proximal C-terminal region and in the S4–S5 linker. Aliphatic chains occupy a hydrophobic pocket between voltage-sensor modules. Overall, this disposition may allow PIP_2 to influence voltage-sensing properties of TRPV channels, as has been suggested recently (30). This PIP_2 interaction with S4–S5 linker charges may affect the flexibility of the region, and in doing so affect the gating properties. Notably, within the first nanosecond of molecular-dynamics simulations that take into account the full system (TRPV1, PIP2, POPC, explicit water, and 140 mM NaCl), the salt bridges reorganized, allowing PIP_2 charges to make periodic contact with Arg-701 but not with Lys-710 (Fig. 4*C*). We observe that Lys-710 is forming a salt bridge that, in our model, appears to be involved in the stabilization of the region, making an intersubunit interaction between proximal and middle portions of C-terminal domains of neighboring subunits (Fig. 4*C*). The strong effect observed when Lys 710 is mutated may possibly be a consequence of a destabilization of a PIP_2-binding site. Because of the structural reorganization we observed after PIP_2 is docked to the channel, it is tempting to suggest the hypothesis that PIP_2 binding modifies salt bridges inside the C-terminal domain working as an on–off switch that regulates channel activity. Moreover, our experiments using chimeras suggest that the effect that PIP_2 exert on TRPM8 and TRPV1 is similar, in both cases, key residues located in the TRP domain are involved in determining the channel PIP_2's apparent affinity. Given these results, it is reasonable to suggest that the coupling between the

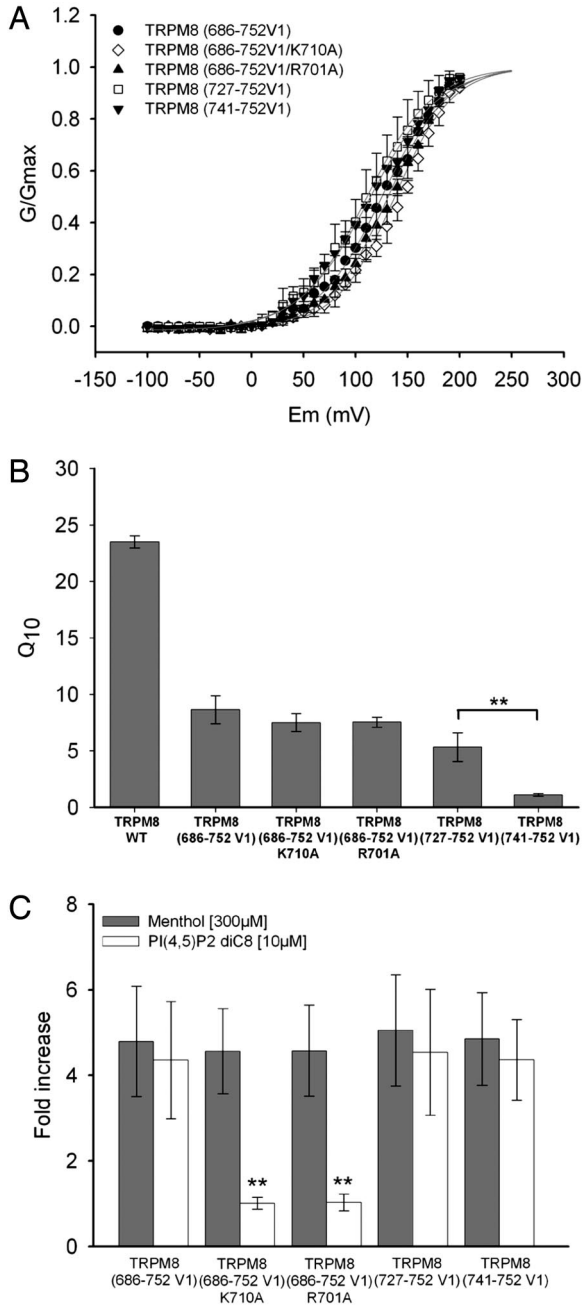

Fig. 3. Voltage-dependence, temperature-dependence and PIP_2 effect on chimeric channels. (*A*) Averaged G/G_{max} vs. V curves for chimeric channels. Solid lines correspond to the best fit to Boltzmann functions. Fit parameters are: V0.5 = 124.96 ± 2 mV, z = 0.83 [TRPM8(686-752V1)]; V0.5 = 137.22 ± 3 mV, z = 0.91 [TRPM8(686-752V1/K710A)]; V0.5 = 130.64 ± 2 mV, z = 0.86 [TRPM8(686-752V1/R701A)];V0.5 = 111.75 ± 2 mV, z = 0.77 [TRPM8(727-752V1)]; V0.5 = 113.04 ± 3 mV, z = 0.75 [TRPM8(741-752V1)]. Each curve represents the average of at least four different experiments performed at 22°C. (*B*) comparative Q_{10} bar plot for the chimeric channels used in this work. Q_{10} was obtained from the ratio of the ionic currents (I) obtained a two different temperatures, $I_T/I_{T+10°C}$ at a fixed voltage. Each bar represents the average of at least four different experiments. Chimeras have a lower Q_{10} (≈10) compared with wild-type TRPM8 (Q_{10} = 23). TRPM8 (741-752 V1) chimera forms temperature-insensitive channels (Q_{10} = 3). (*C*) Effect of PIP_2 (10 μM) and menthol (300 μM). Gray bars indicate menthol, and white bars indicate PIP_2 channel activation. Current records were obtained at +100 mV. Notice that 10 μM PIP_2 is unable to activate the neutralization chimeras. Each point represents an average of at least four different experiments. Error bars indicate SE.

gate and PIP_2-binding site in TRPV1 and TRPM8 is conserved and, most likely, channel architecture is shared on the proximal C-terminal region.

Despite the fact that the possibility that PIP_2 directly inhibits the TRPV1 channel was not explored in the present work, according to our models, an interaction between PIP_2 and the distal portion of TRPV1 channel is very unlikely. The distance from the polar head of PIP_2 and the positive charges existing in the putative inhibitory binding site (amino acids 777–820) is between 20 and 30 Å (Fig. 4 *B* and *D*), discarding a direct interaction as suggested before (13). However, channel inhibition mediated by the site located in the distal portion of the TRPV1 C terminus, whatever its origin, overrides the activating effect of PIP_2 we described herein. The direct addition of PIP_2 on chimerical TRPM8 channels containing the whole C-terminal region of TRPV1 failed to activate the channel but, on the contrary, elicits a modest inhibition of the currents (18). An interpretation of those results would be a down-regulation of the activity of TRPV1 by an indirect action (14, 15).

Separating the Effectors Within the C-Terminal Structure. The complexity we observe in TRP channel regulation demands the presence of a significant number of sensor modules. In this work, we present a dissection of two different regulatory domains within the C-terminal domain, a PIP_2-dependent domain, and a domain responsible for temperature sensitivity (Fig. 4*D*). In addition, we define a small region that confers a thermosensitive phenotype, demonstrating that the role of PIP_2 on temperature gating, if any, is secondary. Moreover, we show that it is possible to eliminate temperature responses of thermoTRP channels and retain their voltage dependency. All these findings strongly suggest that temperature, voltage, and PIP_2 interact allosterically as was hypothesized previously for the case of temperature and voltage gating (31) and for the case of agonist effect and voltage gating (32).

Methods

Molecular Biology. cDNAs coding for rat TRPV1 (GenBank accession no. NM_031982) and rat TRPM8 [kindly provided by David Julius (University of California, San Francisco, CA); GenBank accession no. NM_134371) were used. The boundaries of the transmembrane domains of both channels were defined by consensus by using multiple transmembrane prediction tools. Chimeric thermoTRP channels were made by the overlapping extension method and confirmed by DNA sequencing. DNAs were subcloned into either pCDNA3 or pTracer-CMV2 vectors by using suitable enzymes.

Cell Culture and Transfection. HEK-293 cells were transfected with either pCDNA3 or pTracerCMV2 vectors containing wild-type or chimeric coding DNA sequence. Transfection was carried out by using cationic liposomes, (TransIT-HEK293, Mirus, Madison, WI).

HEK293 Electrophysiology. Whole-cell currents were measured ≈30–40 h after transfection of HEK-293 cells. Gigaseals were formed by using 2–4 MΩ borosilicate pipettes (o.d. = 1.5 mm, i.d. = 0.86 mm, Warner Instruments, Hamden, CT). Whole-cell voltage clamp was performed at various temperatures (10–40°C). The voltage protocol used for all experiments (unless noted) was: hp = 0 mV, membrane was pulsed to voltages between −100 and +200 mV in 10-mV increments of 10-ms duration, followed by a step to −80 mV. Different PIP_2 concentrations were perfused intracellularly through the patch pipette in whole-cell configuration. Normalized conductance (G/G_{max}) was obtained from steady-state current [I (steady-state)/applied voltage] and from tail current when possible. Macroscopic currents were acquired at 100 kHz and filtered at

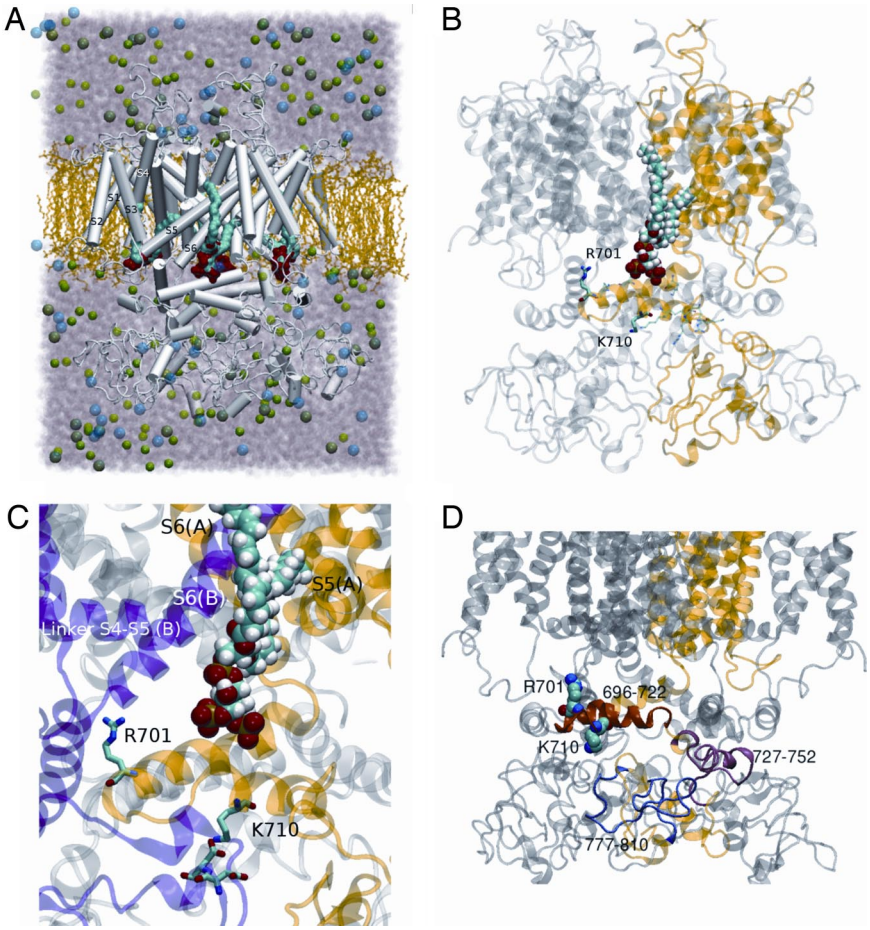

Fig. 4. Homology model for the TRPV1 channel reveals a PIP_2-binding site. (*A*) Side view of the solvated TRPV1–PIP_2-bound channel embedded into a POPC lipid bilayer. Three of the four channel-bound PIP_2 molecules in surface representation can be seen. Blue spheres are Na^+, and green spheres are Cl^- ions (140 mM NaCl). Water molecules (TIP_3) are represented as the transparent red spheres conforming the background. (*B*) Ribbon diagram of the TRPV1 channel depicting one subunit in yellow and one bound PIP_2 molecule. The two positively (R701 and K710) charged amino acid residues involved in the apparent PIP_2 binding are shown in stick representation. Notice the cluster of positively charged residues contained in the proximal part of the C terminus. (*C*) Two channel subunits (purple and yellow) and one PIP_2 molecule are highlighted to describe the interactions between the aliphatic chains and the polar head of PIP_2 with the channel. The aliphatic chains of PIP_2 are making contact with the S6 and S5 transmembrane domains of one subunit [S6(A) and S5(A)] and with the S6 segment of the adjacent subunit [S6(B)]. (*D*) Structures defining the PIP_2 binding (α-helix comprising residues 696–722) and the channel temperature sensitivity (α-helix comprising residues 696–722). Residues 777–810 define the structure proposed as the PIP_2 inhibitory binding site (13).

10 kHz. EPC7 Patch-clamp amplifier (HEKA), 6052E acquisition board (National Instruments, Austin, TX) were used. Data analysis was carried out by using pClamp 9 (Molecular Devices, Sunnyvale, CA) and Origin 7 (Microcal, Northampton, MA).

Solutions. The experiments were done under symmetrical conditions: 140 mM NaCl, 1 mM EGTA, 0.6 mM $Mg\,Cl_2$, and 10 mM Hepes (pH 7.3).

Homology Models and Molecular-Dynamics Simulations. TRPV1 homology models were built by using as reference structure the crystal structures of Kv1.2 (PDB:2A79) (19) and HCN2 (PDB:1Q43) (20) as templates for transmembrane and C-terminal regions, respectively. Multisequence alignment and topology predictions allow an appropriate assignment of the transmembrane region to the model. The transmembrane and C-terminal models were assembled by using the ICM package to build a full model of TRPV1. The intra- and extracellular loops were relaxed by using the Monte Carlo (MC) protocol implemented in ICM. Initial minimization was followed by a short molecular-dynamics (2–5 ps) run to remove initial bad contacts and to fill vacuum pockets. The full model of TRPV1 was used for docking calculations. The lower energy configuration was used to build the complex TRPV1-PIP2, locating symmetrically 4 PIP_2 molecules in the same cavities intermonomers. To relax that system, the model TRPV1-PIP2 was embedded into a POPC lipid bilayer on a water box (TIP3) considering the presence of 140 mM NaCl. The entire system was submitted to a molecular-dynamics simulation under periodic bordering conditions ($124 \times 124 \times 142$). For 1 ns, the full system was relaxed where the backbone atoms of the transmembrane segment and the K^+ ions were restrained by using a harmonic force constant of 5 kcal/mol$Å^2$. Extracellular loops were left free during relaxations. Then a 5-ns simulation was run without restraints. All MD simulations were done by using NAMD with the force field charmm27. The topology file of the PIP_2 molecule was done by adapting the bond parameters available in charmm27. Partial charges were calculated by using the approach ESP with the package Gaussina03. The assembly of the system and figures for the models were done by using the VMD program (33). The PDB file of the full model, topology file of PIP_2, and movies are available at http://cbsm.utalca.cl/cecs/files/trpv1_model.html.

We thank D. Clapham, S. Ramsey, and H. Xu for their suggestions and criticism during the preparation of this work; W. Gonzalez for assistance

in molecular modeling; and P. Devitt for help with the manuscript. This work was supported by the Fondo Nacional de Investigacion Cientifica y Tecnologica (R.L., F.G.-N., and G.O.) and PBCT ACT/24 (F.G.-N.). Centro de Estudios Cientificos is funded in part by grants from Fundación Andes and the Tinker Foundation and hosts a Millennium Science Institute (MIDEPLAN, Chilean Government).

1. Hilgemann D, Feng S, Nasuhoglu C (2001). *Sci STKE* 2001:RE19.
2. McLaughlin S, Murray D (2005) *Nature* 438:605–611.
3. Suh B, Hille B (2005) *Curr Opin Neurobiol* 15:370–378.
4. Runnels L, Yue L, Clapham D (2002) *Nat Cell Biol* 4:329–336.
5. Liu D, Liman E (2003) *Proc Natl Acad Sci USA* 100:15160–15165.
6. Liu B, Qin F (2005) *J Neurosci* 25:1674–1681.
7. Rohacs T, Lopes C, Michailidis I, Logothetis D (2005) *Nat Neurosci* 8:626–634.
8. Lee J, Cha S, Sun T, Huang C (2005) *J Gen Physiol* 126:439–451.
9. Zhang Z, Okawa H, Wang Y, Liman E (2005) *J Biol Chem* 280:39185–39192.
10. Clapham D (2003) *Nature* 426:517–524.
11. Rohacs T (2007) *Pflugers Arch* 453:753–762.
12. Chuang H, Prescott E, Kong H, Shields S, Jordt S, Basbaum A, Chao M, Julius D (2001) *Nature* 411:957–962.
13. Prescott E, Julius D (2003) *Science* 300:1284–1288.
14. Zhang X, Huang J, McNaughton P (2005) *EMBO J* 24:4211–4223.
15. Stein AT, Ufret-Vincenty CA, Hua L, Santana LF, Gordon SE (2006) *J Gen Physiol* 128:509–522.
16. Bandell M, Dubin A, Petrus M, Orth A, Mathur J, Hwang S, Patapoutian A (2006) *Nat Neurosci* 9:493–500.
17. Voets T, Owsianik G, Janssens A, Talavera K, Nilius B (2007) *Nat Chem Biol* 3:35–44.
18. Brauchi S, Orta G, Salazar M, Rosenmann E, Latorre R (2006) *J Neurosci* 26:4835–4840.
19. Long S, Campbell E, MacKinnon R (2005) *Science* 309:897–903.
20. Zagotta W, Olivier N, Black K, Young E, Olson R, Gouaux E (2003) *Nature* 425:200–205.
21. Grottesi A, Domene C, Haider S, Sansom MSP (2005) *IEEE Trans Nanobioscience* 4:112–120.
22. Chatelain FC, Alagem N, Xu Q, Pancaroglu R, Reuveny E, Minor DLJ (2005) *Neuron* 47:833–843.
23. Ferrer-Montiel A, Garcia-Martinez C, Morenilla-Palao C, Garcia-Sanz N, Fernandez-Carvajal A, Fernandez-Ballester G, Planells-Cases R (2004) *Eur J Biochem* 271:1820–1826.
24. Vlachova V, Teisinger J, Susankova K, Lyfenko A, Ettrich R, Vyklicky L (2003) *J Neurosci* 23:1340–1350.
25. Garcia-Sanz N, Fernandez-Carvajal A, Morenilla-Palao C, Planells-Cases R, Fajardo-Sanchez E, Fernandez-Ballester G, Ferrer-Montiel A (2004) *J Neurosci* 24:5307–5314.
26. Montell C (2005). *Sci STKE* 2005:RE3.
27. Ramsey I, Delling M, Clapham D (2006) *Annu Rev Physiol* 68:619–647.
28. Kedei N, Szabo T, Lile JD, Treanor JJ, Olah Z, Iadarola M, Blumberg P (2001) *J Biol Chem* 276:28613–28619.
29. Hoenderop J, Voets T, Hoefs S, Weidema F, Prenen J, Nilius B, Bindels R (2003) *EMBO J* 22:776–785.
30. Nilius B, Mahieu F, Karashima Y, Voets T (2007) *Biochem Soc Trans* 35:105–108.
31. Brauchi S, Orio P, Latorre R (2004) *Proc Natl Acad Sci USA* 101:15494–15499.
32. Nilius B, Talavera K, Owsianik G, Prenen J, Droogmans G, Voets T (2005) *J Physiol* 567:35–44.
33. Humphrey W, Dalke A, Schulten K (1996) *J Mol Graphics* 14:27–28.